PROCEEDINGS OF
THE ROYAL SOCIETY B
BIOLOGICAL SCIENCES

Maximum CO_2 diffusion inside leaves is limited by the scaling of cell size and genome size

Journal:	*Proceedings B*
Manuscript ID	RSPB-2020-3145
Article Type:	Research
Date Submitted by the Author:	17-Dec-2020
Complete List of Authors:	Théroux-Rancourt, Guillaume; University of Natural Resources and Life Sciences Vienna, Institute of Botany Roddy, Adam; Florida International University, Institute of Environment, Department of Biological Sciences Earles, Mason; University of California Davis, Department of Viticulture & Enology; University of California Davis, Department of Biological & Agricultural Engineering Gilbert, Matthew; University of California Davis, Department of Plant Sciences Zwieniecki, Maciej; University of California Davis, Department of Plant Sciences Boyce, Charles; Stanford University, Geological & Environmental Sciences Tholen, Danny; University of Natural Resources and Life Sciences Vienna, Institute of Botany McElrone, Andrew; University of California Davis, Department of Viticulture & Enology; USDA Agricultural Research Service Simonin, Kevin; San Francisco State University, Brodersen, Craig; Yale University Yale School of Forestry and Environmental Studies,
Subject:	Plant science < BIOLOGY, Environmental Science < BIOLOGY, Evolution < BIOLOGY
Keywords:	vascular plants, leaf mesophyll, intercellular airspace, gas diffusion, leaf anatomy
Proceedings B category:	Ecology

Author-supplied statements

Relevant information will appear here if provided.

Ethics

Does your article include research that required ethical approval or permits?:
This article does not present research with ethical considerations

Statement (if applicable):
CUST_IF_YES_ETHICS :No data available.

Data

It is a condition of publication that data, code and materials supporting your paper are made publicly available. Does your paper present new data?:
Yes

Statement (if applicable):
Data is available as Supplemental Tables for microCT data (Supplementary Table S1) and for literature data (Supplementary Table S3). Code to generate the theoretical conductance values is provided as a R script. Segmented microCT images will be made publicly available upon publication on Zenodo at doi:10.5281/zenodo.3606064.

Conflict of interest

I/We declare we have no competing interests

Statement (if applicable):
CUST_STATE_CONFLICT :No data available.

Authors' contributions

This paper has multiple authors and our individual contributions were as below

Statement (if applicable):
GTR, JME, and CRB planned the project, building from ideas of CKB and MJZ, and with contribution from CKB, MJZ, and MEG. GTR, JME, ABR, CRB, AJM, CKB, MJZ, and DT acquired microCT data. GTR and JME segmented the microCT images and extracted data from them. GTR and ABR planned the analysis, analysed the data and created the simulated dataset. KAS collected plant material and prepared samples for genome size analysis. DT contributed finite element modelling. GTR, ABR, KAS, and CRB wrote the manuscript, with contributions from all authors. All authors approved the final version.

Maximum CO_2 diffusion inside leaves is limited by the scaling of cell size and genome size

Guillaume Théroux-Rancourt[a1*], Adam B. Roddy[b1*], J. Mason Earles[c,d], Matthew E. Gilbert[e], Maciej A. Zwieniecki[e], C. Kevin Boyce[f], Danny Tholen[a], Andrew J. McElrone[c,g], Kevin A. Simonin[h], Craig R. Brodersen[i]

[a]Institute of Botany, University of Natural Resources and Life Sciences, 1180 Vienna, Austria
[b]Institute of Environment, Department of Biological Sciences, Florida International University, Miami FL, 33199, USA
[c]Department of Viticulture & Enology, University of California, Davis, CA 95616 USA
[d]Department of Biological & Agricultural Engineering, University of California, Davis, CA 95616 USA
[e]Department of Plant Sciences, University of California, Davis, CA 95616 USA
[f]Department of Geological Sciences, Stanford University, Palo Alto, CA 94305 USA
[g]USDA-Agricultural Research Service, Davis, CA 95616 USA
[h]Department of Biology, San Francisco State University, San Francisco CA 94132 USA
[i]School of the Environment, Yale University, New Haven CT 06511 USA

[1] These authors contributed equally to this work.
* Co-corresponding authors.

Keywords

vascular plants, leaf mesophyll, intercellular airspace, gas diffusion

Abstract

Maintaining high rates of photosynthesis in leaves requires efficient movement of CO_2 from the atmosphere to the mesophyll cells inside the leaf where CO_2 is converted into sugar. CO_2 diffusion inside the leaf depends directly on the structure of the mesophyll cells and their surrounding airspace, which have been difficult to characterize because of their inherently three-dimensional organization. Yet, faster CO_2 diffusion inside the leaf was likely critical in elevating rates of photosynthesis that occurred among angiosperm lineages. Here we characterize the three-dimensional surface area of the leaf mesophyll across vascular plants. We show that genome size determines the sizes and packing densities of cells in all leaf tissues and that smaller cells enable more mesophyll surface area to be packed into the leaf volume, facilitating higher CO_2 diffusion. Measurements and modelling revealed that the spongy mesophyll layer better facilitates gaseous phase diffusion while the palisade mesophyll layer better facilitates liquid phase diffusion. Our results demonstrate that genome downsizing among the angiosperms was critical to restructuring the entire pathway of CO_2 diffusion into and through the leaf, maintaining high rates of CO_2 supply to the leaf mesophyll despite declining atmospheric CO_2 levels during the Cretaceous.

Introduction

The primary limiting enzyme in photosynthesis, rubisco, functions poorly under low CO_2 concentrations. For leaves to sustain high rates of photosynthesis, they must maintain high rates of CO_2 supply from the atmosphere to the sites of carboxylation in the leaf mesophyll. The importance of maintaining efficient CO_2 diffusion into the leaf is reflected in the evolutionary history of leaf anatomy; leaf surface conductance has increased during periods of declining atmospheric CO_2 concentration [1], primarily due to increasing the density and reducing the sizes of stomatal guard cells that form the pores in the epidermis through which CO_2 diffuses [2–5]. However, allowing CO_2 to diffuse into the leaf exposes the wet internal leaf surfaces to a dry atmosphere. Therefore, maintaining a high rate of CO_2 uptake necessarily requires high fluxes of water to be delivered throughout the leaf to replace water lost during transpiration (Supplementary Fig. S1), which is accomplished by a dense network of leaf veins [6,7]. Coordinated increases in the densities of leaf veins and stomata, and reductions in stomatal guard cell size, enabled the elevated photosynthetic rates that occurred only among angiosperm lineages despite declining atmospheric CO_2 concentration during the Cretaceous [1,5,8–13].

For a given leaf volume, the number of cells that can be packed into a space and the distance between different cell types is fundamentally limited by the size of these cells [12,14]. Because cells occupy physical space and increasing investment in any one cell type will displace other cell types [15,16], reducing cell size is hypothesized to be the primary way of allowing more cell types and more cell surface area of a given type to be packed into a given leaf volume. Thus, factors that limit the minimum size of cells represent fundamental constraints on the cellular organization of leaves. While numerous environmental, physiological, and genetic factors can influence the final sizes of somatic cells, the minimum size of a cell is limited by the volume of its nucleus, which is commonly measured as genome size [17–20]. Experimental tests of the effects of genome size on cell size have shown that doubling genome size by arresting mitosis results in larger

and less abundant stomata and mesophyll cells [20–22]. Reductions in cell size and increases in cell packing densities that occurred for veins and stomata only among angiosperm lineages, therefore, required reductions in genome size [13]. While reducing cell size and increasing cell packing density elevate maximum stomatal conductance to CO_2 [4,13], realizing the potential benefits of elevated stomatal conductance to CO_2 diffusion would require modifications to the internal leaf structure that most limits CO_2 transport: the absorptive mesophyll cell surface area exposed to the intercellular airspace.

Diffusion of CO_2 inside the leaf is a major limitation to photosynthesis [23,24] and has been considered to be a prime target for selection to increase photosynthetic capacity [25]. Unlike other tissues, the mesophyll is defined by its intercellular airspace as much as by the cells themselves, both of which determine the overall CO_2 conductance of the tissue. The conductance of the intercellular airspace (g_{ias}) is thought to be much higher than the liquid phase conductance (g_{liq}) through the cell walls, cell membranes, and into the chloroplast stroma [26,27] because CO_2 diffusivity is approximately 10,000 times higher in air than in water. These two conductances are arranged roughly in series, with g_{liq} acting as a greater limitation to CO_2 uptake. While multiple membrane [24] and intracellular factors such as carbonic anhydrase activity [28] and chloroplast positioning [29] can be actively controlled to rapidly change g_{liq} over short timescales, once a leaf is fully expanded, the structural determinants of g_{ias} and g_{liq}, which include the sizes and configurations of cells and airspace in the mesophyll, are thought to be relatively fixed [24,25,30]. Of the various structural determinants of g_{liq} [30], the three-dimensional (3D) surface area of the mesophyll exposed to the intercellular airspace (SA_{mes}) is thought to be the most important because it defines the maximum amount of chloroplast surface area that can line the cell walls [26,27]. Because variation in leaf and mesophyll thicknesses influences SA_{mes} per leaf area [31], expressing SA_{mes} instead by tissue volume (V_{mes}, i.e. the sum of the mesophyll cell volume, V_{cell}, and the airspace volume, V_{air}) accounts for variation in leaf construction [32,33]. The surface area of the mesophyll per tissue volume (SA_{mes}/V_{mes}; Supplementary Fig. S2), therefore, is the primary tissue-level

106 structural trait limiting CO_2 diffusion from the intercellular airspace into the
107 hydrated cell walls of the mesophyll.

108 Because smaller cells have a higher surface area per volume than larger cells,
109 reducing cell size by genome downsizing would allow for more surface area per
110 cell volume (SA_{cell}/V_{cell}) and per total tissue volume (SA_{mes}/V_{mes}) that results in an
111 increase in available diffusive area and the potential for higher rates of CO_2
112 supply to the chloroplasts lining the cell walls. We hypothesized that the cell sizes
113 and packing densities of all cell types in a leaf are fundamentally constrained by
114 genome size [4,5,12,13,19–21,34]. Specifically, we predicted that genome size
115 limits minimum cell size such that smaller genomes allow for a larger range of
116 final cell size in tissues throughout the leaf. Similarly, because more cells can be
117 packed into a given space if these cells are smaller, we predicted that smaller
118 genomes would also allow for higher cell packing densities and greater variation
119 in cell packing densities. Thus, we predicted that the simple requirement that a
120 cell contain its genome would affect cell sizes and cell packing densities of all cell
121 types in the leaf, thereby influencing tissue-level structure and function. In this
122 way, genome downsizing was predicted to allow for smaller cells and higher cell
123 packing densities not only of veins and stomata but also in the mesophyll. The
124 elevated SA_{mes}/V_{mes} enabled by smaller mesophyll cells is predicted to have
125 been an essential innovation among early angiosperms that enabled their
126 elevated rates of CO_2 supply to the photosynthesizing mesophyll cells despite
127 declining atmospheric CO_2 concentrations during the Cretaceous [1,5,8–
128 11,13,20,35,36].

129 We tested these hypotheses using high resolution, 3D X-ray microcomputed
130 tomography (microCT) to characterize cell sizes, cell packing densities, and the
131 exposed 3D surface area of the mesophyll tissue of leaves spanning the extant
132 diversity of vascular plants (Supplementary Table S1). To test how these
133 anatomical innovations in the leaf mesophyll influence CO_2 diffusion, we
134 modelled g_{ias} and g_{liq} as a function of cell size and porosity. The mesophyll tissue
135 of most leaves is composed of two distinct layers, the palisade and the spongy

mesophyll, which are thought to be optimized for different functions [37,38]. We analysed these two layers separately to determine how differences in their 3D tissue structure (Supplementary Figs. S1 and S2) may drive differences in g_{ias} and g_{liq}.

Results and Discussion

Genome downsizing enables re-organization of the leaf mesophyll

For 86 species spanning the extant diversity of vascular plants (Supplementary Table S1), we quantified from microCT images the sizes of spongy and palisade mesophyll cells and stomatal guard cells, as well as the packing densities per unit leaf area of veins, stomata, and palisade mesophyll cells. We first tested whether genome size limited the volumes and packing densities of stomatal guard cells and palisade mesophyll cells by comparing them to published measurements of meristematic cell volume as a function of genome size (Fig. 1) [19]. The shapes of palisade mesophyll cells and stomatal guard cells can be approximated as capsules, such that cell volumes can be calculated from linear dimensions of length or diameter (see Methods) [20,39]. Mature plant cells are always larger than their meristematic precursors, often considerably larger (Fig. 1a,b) [19–21,34]. By reducing the size of meristematic cells, genome downsizing allows for smaller minimum cell size and also a greater range in mature cell size of both stomatal guard cells and palisade mesophyll cells (Fig. 1a), consistent with prior results [13,20]. These effects of genome size on cell size were also reflected in the packing densities of guard cells and palisade mesophyll cells (Fig. 1c,d). Smaller genomes raised the upper limit on maximum packing densities of meristematic cells, allowing for higher packing densities of both guard cells (D_{stom}) and palisade mesophyll cells ($D_{palisade}$), consistent with prior results for veins, stomata [13,22], and mesophyll cells [21,34]. Not only did smaller genomes result in smaller cells and higher cell packing densities, but smaller

genomes also allowed for greater variation in cell sizes and cell packing densities of stomata, mesophyll, and veins (Fig. 1a,c and Supplementary Fig. S3) [13,20,40]. The shapes of stomatal guard cells and palisade mesophyll cells are regular enough to allow cell volume and surface area to be predicted from linear dimensions, but the shapes of spongy mesophyll cells are irregular and highly lobed. As a consequence, spongy mesophyll cell volume cannot be easily calculated from a single linear dimension. To extend these analyses to the spongy mesophyll we tested whether linear cell dimensions were predicted by genome size, as has been shown for guard cell length [40]. Genome size was a strong predictor of cell diameters of stomatal guard cells, palisade mesophyll cells, and spongy mesophyll cell lobes (Supplementary Table S2 and Fig. S3). We found no relationship between genome size and mesophyll porosity (Supplementary Figs. S3 and S4), which is the volumetric airspace fraction of the leaf, likely because many combinations of cell sizes and packing densities can result in the same porosity [41]. Despite the role of porosity in facilitating diffusion in the intercellular airspace [42], traits related to cellular organization within the mesophyll are likely to have a greater influence than porosity on the diffusive conductance of CO_2 through the intercellular airspace and into the photosynthetic mesophyll cells [33].

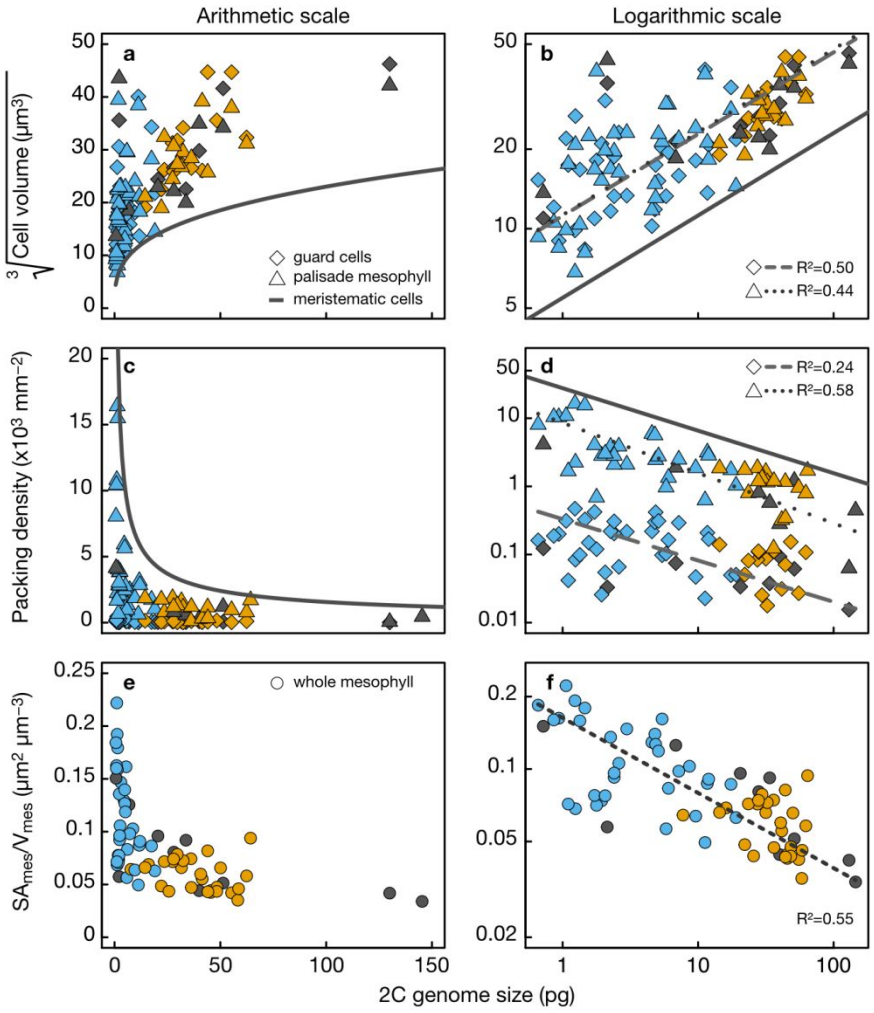

Fig. 1. *(a,b) Cell volumes, (c,d) cell packing densities, and (e,f) total mesophyll surface area per tissue volume (SA_{mes}/V_{mes}) in leaves scale with 2C genome size across vascular plants (angiosperms, blue; gymnosperms, orange; ferns and fern allies, grey). Minimum cell volumes (modelled from cell diameters) and maximum cell packing densities are limited by the size of meristematic cells (solid lines). Measurements of meristematic cells as a function of genome size in log-log space (b, solid line; from [19]) are reproduced in arithmetic space (a). Theoretical maximum packing density of meristematic cells (c,d) was calculated from measured cell volumes [19] as the reciprocal of meristematic cell cross-sectional area (see Methods) assuming spherically shaped cells.*

Because cell surfaces can be in contact with other cells and be unavailable for CO_2 absorption, we tested whether the effect of genome size extends beyond limiting the sizes and packing densities of cells to influencing the surface area of the mesophyll tissue exposed to the intercellular airspace (SA_{mes}). Genome size was a strong predictor of the total surface area per tissue volume of the mesophyll cells exposed to the intercellular airspace, SA_{mes}/V_{mes} (Fig. 1e,f and Supplementary Table S2), which is the anatomically fixed component of the leaf mesophyll that influences CO_2 diffusion. Our results suggest that except for a few ferns with small genomes, only angiosperms have been able to build leaves with high SA_{mes}/V_{mes} (Fig. 2a). To explore this prediction beyond our dataset, we combined new measurements of SA_{mes}/V_{mes} on the species for which we had microCT images with data extracted from the literature for 85 additional species (Fig. 2a and Supplementary Table S3). The distribution of SA_{mes}/V_{mes} among clades in our dataset was consistent with the data extracted from the literature and showed that the highest and most variable SA_{mes}/V_{mes} occur only among monocots and eudicots, suggesting that anatomical innovations among the angiosperms are responsible for the heightened SA_{mes}/V_{mes} necessary to support high rates of photosynthesis. To test the prediction that genome downsizing enabled high SA_{mes}/V_{mes} (Fig. 1e,f) via impacts on cell size and cell packing density, we tested whether SA_{mes}/V_{mes} was coordinated with the sizes and packing densities of cells and tissues throughout the leaf. The packing densities of stomata, veins, and palisade mesophyll cells were all strongly and positively related to SA_{mes}/V_{mes} (Fig. 2b-d), while the diameters of stomatal guard cells and of spongy and palisade mesophyll cells were all strongly and negatively related to SA_{mes}/V_{mes} (Fig. 2e-g). This whole-leaf trade-off between cell size and cell packing density (Fig. 1, S4) was apparent in multidimensional space, in which the first axis was aligned with genome size and explained the majority of the variation whether or not phylogenetic covariation was included (Supplementary Fig. S5). While small genomes, small cells, and high SA_{mes}/V_{mes} occur predominantly among the angiosperms, some xerophytic ferns, as well as the lycophyte *Selaginella kraussiana*, also share these traits. The repeated co-occurrence of

these traits among different clades and the statistically significant phylogenetic regressions between genome size, cell sizes and packing densities, and SA_{mes}/V_{mes} (Supplementary Table S2 and Fig. S5) further corroborate the role of genome size in determining the sizes and arrangement of cells and tissues throughout the leaf that enable high fluxes of CO_2 and H_2O across the leaf epidermis.

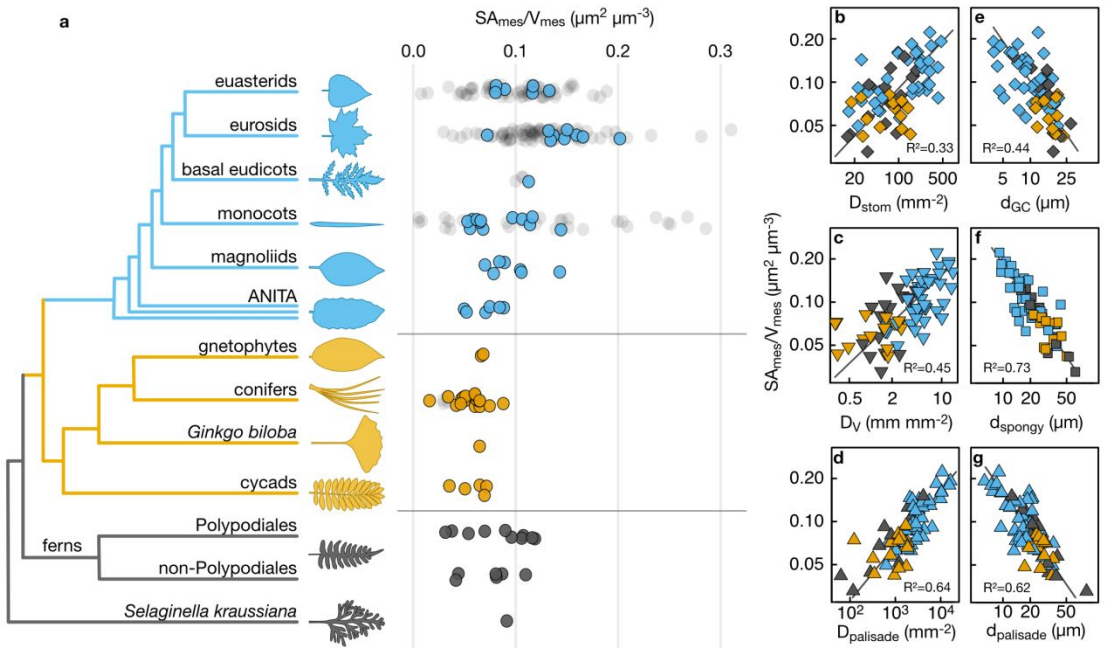

Fig. 2. *Mesophyll surface area per mesophyll volume (SA_{mes}/V_{mes}) scales with cell size, cell packing densities, and 2C genome size across vascular plants. (a) Distribution of SA_{mes}/V_{mes} across 86 species of terrestrial vascular plants (coloured points) compared to values computed from the literature (shaded grey dots, 81 angiosperms and four gymnosperms; see Supplemental Methods). Packing densities of (b) stomata on the leaf surface (D_{stom}), (c) veins (D_V), and (d) palisade mesophyll cells ($D_{palisade}$) all scaled positively with SA_{mes}/V_{mes} while the diameters of (e) stomatal guard cells (d_{GC}), (f) spongy mesophyll cells (d_{spongy}), and (g) palisade mesophyll cells ($d_{palisade}$) all scaled negatively with SA_{mes}/V_{mes}. Solid lines represent standardized major axes. All bivariate relationships remained highly significant after accounting for shared evolutionary history (Supplementary Table S2).*

Increasing liquid phase conductance optimizes the entire diffusive pathway

While light is intercepted primarily by the upper palisade mesophyll layer [37], CO_2 enters the leaf on the lower spongy mesophyll layer for most terrestrial plants, creating opposing gradients of two of the primary reactants in photosynthesis. Within a leaf, the spongy and palisade layers have divergent cell shapes and organizations that are thought to accommodate these opposing gradients by facilitating CO_2 diffusion in the gaseous and liquid phases. Both cell size and porosity can affect SA_{mes}/V_{mes} and the diffusive conductances (g_{ias} and g_{liq}) that are considered targets of selection to increase photosynthesis [20,31,38,41,42]. To determine whether cell size or porosity has a greater effect on SA_{mes}/V_{mes} and on modelled g_{ias}, and g_{liq}, we measured cell diameter, porosity, and SA_{mes}/V_{mes} for the spongy and palisade layers separately for 47 species in our dataset, encompassing all major lineages of vascular plants.

The scaling of cell diameter with SA_{mes}/V_{mes} (Fig. 2e-g) suggested that cell diameter would have a greater impact than porosity on SA_{mes}/V_{mes}. Smaller cells have a higher ratio of surface area to volume, an effect that could propagate up to influencing SA_{mes}/V_{mes} of the entire tissue. In contrast, we predicted that porosity would not have a consistent impact on SA_{mes}/V_{mes} because at very low porosities there is very little cell surface area exposed to the airspace while at very high porosities there is very little cell surface area relative to a large volume of tissue. Consistent with these predictions, decreasing cell size led to higher SA_{mes}/V_{mes} across species and mesophyll layers, and variation in porosity had no consistent effect on SA_{mes}/V_{mes} (Fig. 3). Rather, both low (<0.1) and high (>0.6) porosities led to lower SA_{mes}/V_{mes}. This conditional effect of porosity on SA_{mes}/V_{mes} suggests that there is a relatively narrow range of porosities that allows for simultaneous optimization of g_{liq} and g_{ias} in C3 plants. However, the strong and consistent effect of reducing cell size on increasing SA_{mes}/V_{mes} among species and among mesophyll tissues within a leaf further implicates cell size

and, by extension, genome size in controlling cell- and tissue-level traits responsible for increasing the CO_2 conductance of the mesophyll.

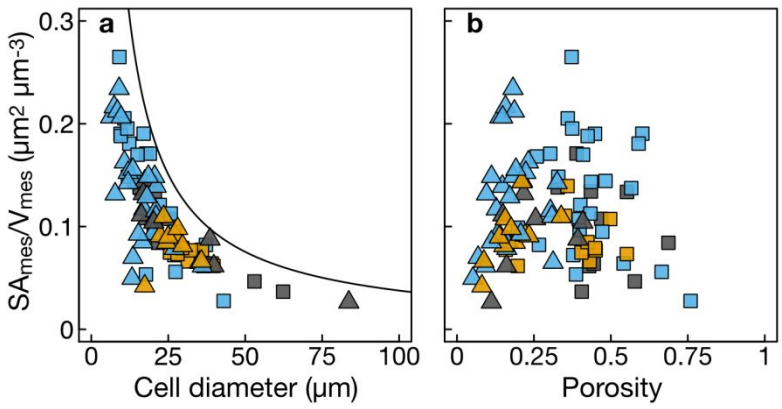

Fig. 3. *The effects of cell size and porosity on 3D mesophyll surface per mesophyll volume (SA_{mes}/V_{mes}). (a) Smaller cells in both the palisade (triangles) and spongy (squares) mesophyll are associated with higher SA_{mes}/V_{mes}. The solid line represents the theoretical maximum SA_{mes}/V_{mes} calculated from the densest packing of cylinders in a rectangular volume (porosity of approximately 0.09 m^3 m^{-3}). (b) SA_{mes}/V_{mes} was highest at intermediate porosity because the highest possible porosity can occur only when there are no cells and the lowest porosity occurs when all cells are in complete contact and there is no airspace. Points are coloured by plant clade, according to Fig. 2.*

To test how these anatomical traits affect g_{ias} and g_{liq}, we compared modelled estimates of g_{ias} and g_{liq} per unit leaf volume [24,33], in which cell size and porosity were varied independently, to measurements of cell diameter and mesophyll porosity taken from microCT images for the two mesophyll layers. Although this modelling did not incorporate adjustments that can alter g_{liq} over short timescales, it nonetheless shows how variation in anatomy, which is relatively fixed once a leaf has expanded [24], can influence g_{ias} and g_{liq}. Based on simple packing of capsules, we predicted that increasing volumetric g_{liq} would

occur primarily by decreasing cell size, while increasing volumetric g_{ias} would occur primarily by increasing porosity. We also predicted that the palisade layer, whose densely packed columnar cells channel light deep into the leaf much as a fibre optic cable directs light [37], would be optimized for g_{liq} rather than for g_{ias} in order to deliver CO_2 efficiently to the places where light is abundant. In contrast, we predicted that the spongy mesophyll layer would be optimized for high g_{ias} in order to promote gaseous CO_2 diffusion into the upper palisade layer [23] while also scattering and absorbing light [43].

Our analysis confirmed that cell size and porosity have different effects on modelled volumetric estimates of g_{liq} and g_{ias} (background shading in Fig. 4). While increasing porosity leads to higher g_{ias}, it has a relatively small effect on g_{liq} for a given cell size. In contrast, increasing g_{liq} predominantly occurs by reducing cell size, which has only a moderate effect on g_{ias} and only when porosity is relatively high. Additionally, for a given cell size, increasing porosity reduces g_{liq}. Thus, reductions in cell size increase both g_{liq} and g_{ias}, but increasing porosity has opposite effects on g_{liq} and g_{ias}. As predicted, our measurements showed that the palisade layer had lower porosities that are associated with higher g_{liq}, while the spongy layer had higher porosities that are associated with higher g_{ias} (Fig. 4 and Supplementary Figs. S12-S14). This specialization of the two layers reflects the need to maintain a high g_{ias} in the spongy mesophyll where CO_2 is abundant to promote its diffusion into the palisade and the need to maintain high g_{liq} in the palisade mesophyll where light is abundant to promote liquid-phase diffusion of CO_2 into the cell walls (Supplementary Figs. S6 and S8). Many species, particularly angiosperms, have palisade mesophyll characterized by small, highly packed cells that allow volumetric g_{liq} to be higher than g_{ias} of this tissue (Figs. 1, 4 and Supplementary Fig. S4). This pattern suggests that CO_2 fixation in the palisade may be limited by the gaseous supply of CO_2 and not by its liquid-phase diffusion into cells, consistent with prior reports for hypostomatous leaves that the majority of CO_2 fixation occurs not at the top of the leaf where CO_2 is unlikely to penetrate but deeper in the palisade [43]. The

325 structure and organization of palisade and spongy layers of the mesophyll
326 therefore reflect the relative strengths of the opposing gradients of CO_2 and light.

327

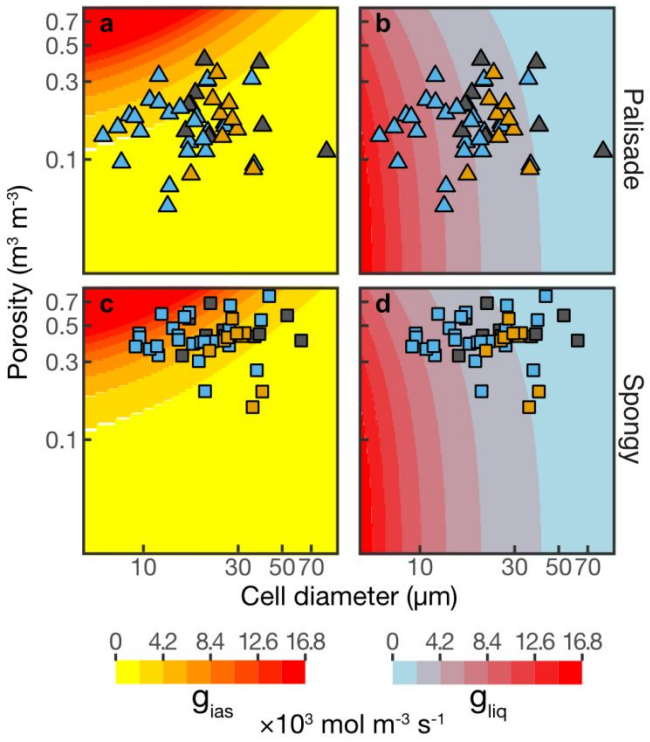

328

329 ***Fig. 4.*** *Distribution of observed cell sizes and porosities for (a,b) palisade and*
330 *(c,d) spongy mesophyll relative to modelled estimates of (a,c) airspace*
331 *conductance (g_{ias}) and (b,d) liquid phase conductance (g_{liq}) to CO_2. Measured*
332 *values of cell size and porosity (points) are plotted over theoretical conductances*
333 *(coloured shading) estimated by simulating leaves of varying cell diameter and*
334 *porosity (see Supplementary Methods). Points are coloured by plant clade,*
335 *according to Fig. 2.*

Concluding remarks

Our results suggest that the heightened rates of leaf-level gas exchange that occurred predominantly among angiosperms are coordinated with changes not only in veins and stomata [1,5,8,9,12,13] but also in the three-dimensional organization of the leaf mesophyll tissues that limit the exchange of CO_2 and water. Although coordinating changes in veins, stomata, and the mesophyll undoubtedly involves multiple molecular developmental programs, the scaling of genome size and cell size emerged as the predominant factor driving the increase in SA_{mes}/V_{mes} and g_{liq} that together enabled higher rates of CO_2 movement into the photosynthetic mesophyll cells. While the size and abundance of chloroplasts in the leaf will undoubtedly affect photosynthetic rates, the maximum chloroplast surface area available for CO_2 diffusion is limited by the surface area of the mesophyll. Because photosynthetic metabolism is the primary source of energy and matter for the biosphere, leaf-level processes are directly linked to ecological processes globally [3]. Yet, theory linking ecosystem processes to organismal level metabolism has focused predominantly on the structure of vascular supply networks [44,45]. Our results suggest that the scaling of photosynthetic metabolism with resource supply networks extends beyond the vascular system and into the photosynthetic cells of the leaf mesophyll where energy and matter are exchanged. Moreover, these results highlight the critical role of cell size in defining maximum rates of leaf gas exchange [20,46], in contrast to assumptions in current theory that terminal metabolic units are size-invariant [47,48]. Incorporating the structure of the mesophyll tissue into theory linking leaf-level and ecosystem-level processes could improve model predictions of photosynthesis. Furthermore, the physiological benefits of small cells may be one reason why the angiosperms so readily undergo genome size reductions subsequent to genome duplications [13,20,49,50]. While whole genome duplications may drive ecological and evolutionary innovation [51–53], selection for increased photosynthetic capacity subsequent to genome duplication may

drive reductions in both cell size and genome size to optimize carbon fixation, reiterating a role for metabolism in genome size evolution [5,13,20].

Materials and Methods

Plant material

Mature, fully expanded leaves from healthy, well-watered plants were collected from greenhouses, botanical gardens, fields, and other outdoor growing locations to represent a broad phylogenetic diversity of C3 vascular plants (Supplementary Table S1). We chose representative angiosperms from the ANA grade, magnoliids, monocots, basal eudicots, eurosids, and euasterids. We also sampled the lycophyte *Selaginella kraussiana*, 17 species of ferns from 12 families, and major groups of gymnosperms, including gnetophytes, cycads, and conifers. Leaves were cut at the base of the petiole or of short stem segment, immediately put in a plastic bag with the cut end wrapped in paper towels, and scanned within 36 h of excision.

MicroCT data acquisition

MicroCT scanning was carried out at the Advanced Light Source (ALS; beamline 8.3.2; Lawrence Berkeley National Lab, Berkeley, CA, USA), the Swiss Light Source (SLS; TOMCAT Tomography beamline; Paul Scherrer Institute, Villigen, Switzerland), and the Advanced Photon Source (APS; beamline 2-BM-A,B; Argonne National Laboratory, Lemont, IL, USA). Samples were prepared less than 30 min before each scan. For laminar leaves, a ~1.5 to 2-mm-wide and ~15-mm-long piece of leaf was excised between the midrib and the leaf outer edge. For needle and non-laminar leaves, a piece ~15-mm-long was used. Tissue samples were enclosed between Kapton (polyimide) tape to prevent desiccation while allowing high X-ray transmittance. Samples were scanned

using the continuous tomography mode capturing 1,025 (ALS, APS) or 1,800 (SLS) projection images at 21 to 25 keV, using primarily 5x (55 species; pixel size of 1.27 μm) and 10x (29 species; pixel size of 0.64 μm) objective lenses, or a 40x objective lens (2 species; pixel size of 0.1625 μm). Each scan was completed in 5 min to 15 min.

Images were reconstructed using TomoPy [54] for all ALS samples or using the in-house reconstruction platform for SLS or APS samples. Reconstructed scans were processed using published methods [32,55], and image stacks were cropped to remove tissue that was dehydrated, damaged, or contained artifacts from the imaging or reconstruction steps. The final stacks contained ~500-2000 eight-bit grayscale images (downsampled from 16 or 32-bit images).

Leaf trait analysis

Leaf and mesophyll thickness were measured on cross-sectional slices of the image stack. Cell diameter was measured on at least 10 cells for each mesophyll layer on paradermal slices of the stack, as well as for guard cell length and diameter. For spongy mesophyll cells with lobed or irregular shapes, cell diameter was measured on the lobes of the cells and not on their presumed centres [56]. Some leaves had only palisade-like or spongy-like cells, resulting in some species having data for only one cell type (Supplementary Table S1). To estimate cell volume, we assumed stomatal guard cells and palisade mesophyll cells were shaped as capsules with length equal to twice the diameter of the cylinder (e.g. $d_{palisade}$ or d_{GC}), allowing for cell volume to be calculated as [20]:

$$V = \frac{5}{96}\pi(2d)^3.$$

We compared these estimates of mature cell volume to published measurements of meristematic cell volumes as a function of genome size [19]. We used empirical relationships between meristematic cell volume and nuclear volume and between nuclear volume and genome size [19] to estimate the relationship between meristematic cell volume and genome size, consistent with a prior

analysis [20]. To estimate maximum meristematic cell packing densities in 2D, we assumed meristematic cells were shaped as spheres and calculated the maximum packing density (number of cells per area) as one divided by the cross-sectional area of the sphere, following published methods for stomata [4].

Palisade cell packing density in 2D was measured on stacks from paradermal planes through the palisade tissue by averaging per species the counts of palisade cells present within three defined areas. Stomatal density and vein density were measured on the original uncropped image stack to maximize the area measured. Scans in which stomata were difficult to discern or in which vein density would have been obviously biased (e.g. high fraction of the scan containing a higher order vein) were not measured for these traits.

To extract surface area and volumes, mesophyll cells, airspace, vasculature (combined veins and bundle sheath), and background (including the epidermis) were segmented using published methods [32,55] and ImageJ [57]. Airspace (V_{pores}), mesophyll cell (V_{cells}), both summing up to the total mesophyll volume (V_{mes}), vasculature volume (V_{veins}), and the surface area exposed to the intercellular airspace (SA_{mes}) were then extracted using published methods [32] with the ImageJ plugin BoneJ [58], or using a custom Python program [55] (https://github.com/plant-microct-tools/leaf-traits-microct). SA_{mes}/V_{mes} is less sensitive to leaf thickness than the commonly measured S_m, i.e. SA_{mes} per leaf area (Supplemental Figure S8; Supplemental Table S1). For separate quantification of traits from palisade and spongy mesophyll, segmented stacks were cropped at the interface between tissues or where vasculature was present, in order to accurately characterize SA_{mes}, volumes, and cell diameter within those tissues.

Because our sampling included scans made at different magnifications, we tested the effect of magnification on measurements of cell size and SA_{mes} (Supplemental Results). Overall, lower magnification scans resulted in small (less than 5% for most scans) but significant changes in cell diameter and SA_{mes} (Supplemental Fig. S6 and S7). However, reanalysis of scaling relationships

reported in Fig. 2 incorporating this error showed that all relationships remained as significant as those in the original dataset (Supplementary Table S3), suggesting that our results are robust to inclusion of scans with different magnifications. SMA slopes diverged only slightly between magnifications and most often were not significantly different (Supplementary Table S4).

Genome size data

Existing 2C genome size (pg) data available in the Kew Plant DNA C-values Database [59] were matched to the majority of species in our dataset. Fresh leaf samples of species not in the database were collected at the University of California Botanical Garden, Berkeley CA from the same plants imaged. Genome sizes (Supplementary Table S1) were measured by the Benaroya Research Institute, Virginia Mason University, using the *Zea mays* or *Vicia faba* standards and following standard protocols [60].

Simulating conductance data using cell size and porosity

To simulate g_{liq} and g_{ias} (background shading in Fig. 4), we used all possible combinations of cell diameter (5 to 124 μm in 0.1 μm steps; 1 μm below and 40 μm above the range in our data) and porosity (0.02 to 0.96 in 0.01 steps; 0.03 below and 0.01 above the range in our data). For g_{liq}, we approximated cells as capsules [39], with diameter d and height $3d$, and generated the densest lattice possible, consisting of 30 cells in a $(5d)^2$ projected area (Supplementary Fig. S10), with a total volume of $2d$ × projected area and a total porosity of 0.186 (see Supplemental Methods for further details). Simulating porosity above or below 0.186 was done by changing pore volume and keeping cell volume constant, which modified total lattice volume to represent either a looser cell packing or cells inflated and deformed into each other.

Liquid phase conductance per mesophyll volume was computed [24] as a function of the surface area exposed to the intercellular airspace per volume,

itself a function of cell diameter and porosity within the cell lattice, using published values for the different resistance components [24] (see Supplemental Information). For g_{ias}, we accounted for tortuosity and diffusive path lengthening as functions of porosity [33], and mesophyll thickness as a function of cell diameter as observed in our dataset (R^2 = 0.21, p<0.0001; Supplementary Fig. S11).

Statistical analysis

All analyses, simulations, and conductance computations were carried out in R 4.0.3 [61]. Standardized major axes were computed using the smatr package [62], and phylogenetic analyses (reduced major axis, generalized least squares regression, and principal component analysis) are detailed in the Supplementary Methods.

Acknowledgements

We thank the University of California Botanical Garden (Berkeley, CA), the UC Davis Botanical Conservatory (Davis, CA), and the UC Davis Arboretum (Davis, CA) for plant material, the Paul Scherrer Institute, Villigen, Switzerland for provision of synchrotron radiation beam time at beamline TOMCAT. We thank the many who collected plant material on our behalf.

Funding

This work was supported by a Katherine Esau Fellowship to GTR, by the Austrian Science Fund (FWF), projects M2245 and P30275, and US NSF grant DEB-1838327. The Advanced Light Source is supported by the Director, Office of Science, Office of Basic Energy Sciences, of the US Department of Energy under Contract no. DE-AC02-05CH11231.

References

1. Boer HJ de, Eppinga MB, Wassen MJ, Dekker SC. 2012 A critical transition in leaf evolution facilitated the Cretaceous angiosperm revolution. *Nature Communications* **3**, 1221. (doi:10.1038/ncomms2217)

2. Beerling D, Woodward F. 1997 Changes in land plant function over the phanerozoic: Reconstructions based on the fossil record. *Botanical Journal of the Linnean Society* **124**, 137–153.

3. Hetherington AM, Woodward FI. 2003 The role of stomata in sensing and driving environmental change. *Nature* **424**, 901–908.

4. Franks PJ, Beerling DJ. 2009 Maximum leaf conductance driven by CO_2 effects on stomatal size and density over geologic time. *Proceedings of the National Academy of Sciences* **106**, 10343–10347. (doi:10.1073/pnas.0904209106)

5. Franks PJ, Freckleton RP, Beaulieu JM, Leitch IJ, Beerling DJ. 2012 Megacycles of atmospheric carbon dioxide concentration correlate with fossil plant genome size. *Philosophical Transactions of the Royal Society B: Biological Sciences* **367**, 556–564. (doi:10.1098/rstb.2011.0269)

6. Brodribb TJ, Holbrook NM, Zwieniecki MA, Palma B. 2005 Leaf hydraulic capacity in ferns, conifers and angiosperms: Impacts on photosynthetic maxima. *New Phytologist* **165**, 839–846. (doi:10.1111/j.1469-8137.2004.01259.x)

7. Brodribb TJ, Feild TS, Jordan GJ. 2007 Leaf maximum photosynthetic rate and venation are linked by hydraulics. *Plant Physiology* **144**, 1890–1898.

8. Boyce CK, Brodribb TJ, Feild TS, Zwieniecki MA. 2009 Angiosperm leaf vein evolution was physiologically and environmentally transformative. *Proceedings of the Royal Society B: Biological Sciences* **276**, 1771–1776. (doi:10.1098/rspb.2008.1919)

527 9. Brodribb TJ, Feild TS. 2010 Leaf hydraulic evolution led a surge in leaf
528 photosynthetic capacity during early angiosperm diversification. *Ecology Letters*
529 **13**, 175–183.

530 10. Feild TS *et al.* 2011 Fossil evidence for cretaceous escalation in angiosperm
531 leaf vein evolution. *Proceedings of the National Academy of Sciences* **108**, 8363–
532 8366. (doi:10.1073/pnas.1014456108)

533 11. Boyce CK, Zwieniecki MA. 2012 Leaf fossil record suggests limited influence
534 of atmospheric CO_2 on terrestrial productivity prior to angiosperm evolution.
535 *Proceedings of the National Academy of Sciences* **109**, 10403–10408.
536 (doi:10.1073/pnas.1203769109)

537 12. Brodribb TJ, Jordan GJ, Carpenter RJ. 2013 Unified changes in cell size
538 permit coordinated leaf evolution. *New Phytologist* **199**, 559–570.
539 (doi:10.1111/nph.12300)

540 13. Simonin KA, Roddy AB. 2018 Genome downsizing, physiological novelty, and
541 the global dominance of flowering plants. *PLoS Biology* **16**, e2003706.

542 14. John GP, Scoffoni C, Sack L. 2013 Allometry of cells and tissues within
543 leaves. *American Journal of Botany* **100**, 1936–1948.

544 15. Feild TS, Brodribb TJ. 2013 Hydraulic tuning of vein cell microstructure in the
545 evolution of angiosperm venation networks. *New Phytologist* **199**, 720–726.
546 (doi:10.1111/nph.12311)

547 16. Baresch A, Crifò C, Boyce CK. 2019 Competition for epidermal space in the
548 evolution of leaves with high physiological rates. *New Phytologist* **221**, 628–639.

549 17. Mirsky A, Ris H. 1951 The desoxyribonucleic acid content of animal cells and
550 its evolutionary significance. *The Journal of General Physiology* **34**, 451.

551 18. Cavalier-Smith T. 1978 Nuclear volume control by nucleoskeletal DNA,
552 selection for cell volume and cell growth rate, and the solution of the DNA C-
553 value paradox. *Journal of Cell Science* **34**, 247–278.

554 19. Šímová I, Herben T. 2012 Geometrical constraints in the scaling relationships
555 between genome size, cell size and cell cycle length in herbaceous plants.
556 *Proceedings of the Royal Society B: Biological Sciences* **279**, 867–875.
557 (doi:10.1098/rspb.2011.1284)

558 20. Roddy AB *et al.* 2020 The scaling of genome size and cell size limits
559 maximum rates of photosynthesis with implications for ecological strategies.
560 *International Journal of Plant Sciences* **181**, 75–87. (doi:10.1086/706186)

561 21. Francis A, Jones R, Parker J, Posselt U. 1990 Colchicine-induced heritable
562 variation in cell size and chloroplast numbers in leaf mesophyll cells of diploid
563 ryegrass (*Lolium perenne* L.). *Euphytica* **49**, 49–55.

564 22. Mo L, Chen J, Lou X, Xu Q, Dong R, Tong Z, Huang H, Lin E. 2020
565 Colchicine-induced polyploidy in *Rhododendron fortunei* Lindl. *Plants* **9**, 424.
566 (doi:10.3390/plants9040424)

567 23. Parkhurst D. 1986 Internal leaf structure: A three-dimensional perspective. In
568 *On the economy of plant form and function*, Cambridge [Cambridgeshire]:
569 Cambridge University Press, c1986.

570 24. Evans JR, Kaldenhoff R, Genty B, Terashima I. 2009 Resistances along the
571 CO_2 diffusion pathway inside leaves. *Journal of Experimental Botany* **60**, 2235–
572 2248. (doi:10.1093/jxb/erp117)

573 25. Lundgren MR, Fleming AJ. 2020 Cellular perspectives for improving
574 mesophyll conductance. *The Plant Journal* **101**, 845–857.
575 (doi:10.1111/tpj.14656)

576 26. Tomas M *et al.* 2013 Importance of leaf anatomy in determining mesophyll
577 diffusion conductance to CO_2 across species: quantitative limitations and scaling
578 up by models. *Journal of Experimental Botany* **64**, 2269–2281.
579 (doi:10.1093/jxb/ert086)

27. Tosens T *et al.* 2016 The photosynthetic capacity in 35 ferns and fern allies: mesophyll CO_2 diffusion as a key trait. *New Phytologist* **209**, 1576–1590. (doi:10.1111/nph.13719)

28. Momayyezi M, McKown AD, Bell SCS, Guy RD. 2020 Emerging roles for carbonic anhydrase in mesophyll conductance and photosynthesis. *The Plant Journal* **101**, 831–844. (doi:10.1111/tpj.14638)

29. Tholen D, Boom C, Noguchi KO, Ueda S, Katase T, Terashima I. 2008 The chloroplast avoidance response decreases internal conductance to CO_2 diffusion in Arabidopsis thaliana leaves. *Plant, Cell & Environment* **31**, 1688–1700. (doi:10.1111/j.1365-3040.2008.01875.x)

30. Evans JR. In press. Mesophyll conductance: Walls, membranes and spatial complexity. *New Phytologist* **n/a**. (doi:https://doi.org/10.1111/nph.16968)

31. Ren T, Weraduwage SM, Sharkey TD. 2019 Prospects for enhancing leaf photosynthetic capacity by manipulating mesophyll cell morphology. *Journal of Experimental Botany* **70**, 1153–1165. (doi:10.1093/jxb/ery448)

32. Théroux-Rancourt G, Earles JM, Gilbert ME, Zwieniecki MA, Boyce CK, McElrone AJ, Brodersen CR. 2017 The bias of a two-dimensional view: Comparing two-dimensional and three-dimensional mesophyll surface area estimates using noninvasive imaging. *New Phytologist* **215**, 1609–1622. (doi:10.1111/nph.14687)

33. Earles JM, Théroux-Rancourt G, Roddy AB, Gilbert ME, McElrone AJ, Brodersen CR. 2018 Beyond porosity: 3D leaf intercellular airspace traits that impact mesophyll conductance. *Plant Physiology* **178**, 148–162.

34. Hassan L, Wazuddin M. 2000 Colchicine-induced variation of cell size and chloroplast number in leaf mesophyll of rice. *Plant breeding* **119**, 531–533.

35. Beerling DJ, Franks PJ. 2010 The hidden cost of transpiration. *Nature* **464**, 495–496.

607 36. McKown AD, Cochard H, Sack L. 2010 Decoding leaf hydraulics with a
608 spatially explicit model: Principles of venation architecture and implications for its
609 evolution. *The American Naturalist* **175**, 447–460. (doi:10.1086/650721)

610 37. Smith WK, Vogelmann TC, DeLucia EH, Bell DT, Shepherd KA. 1997 Leaf
611 Form and Photosynthesis. *BioScience* **47**, 785–793. (doi:10.2307/1313100)

612 38. Tholen D, Boom C, Zhu X-G. 2012 Opinion: Prospects for improving
613 photosynthesis by altering leaf anatomy. *Plant Science* **197**, 92–101.

614 39. Harwood R, Goodman E, Gudmundsdottir M, Huynh M, Musulin Q, Song M,
615 Barbour MM. 2020 Cell and chloroplast anatomical features are poorly estimated
616 from 2D cross-sections. *New Phytologist* **225**, 2567–2578.
617 (doi:10.1111/nph.16219)

618 40. Beaulieu JM, Leitch IJ, Patel S, Pendharkar A, Knight CA. 2008 Genome size
619 is a strong predictor of cell size and stomatal density in angiosperms. *New*
620 *Phytologist* **179**, 975–986.

621 41. Lehmeier C *et al.* 2017 Cell density and airspace patterning in the leaf can be
622 manipulated to increase leaf photosynthetic capacity. *The Plant Journal* **92**, 981–
623 994. (doi:10.1111/tpj.13727)

624 42. Lundgren MR *et al.* 2019 Mesophyll porosity is modulated by the presence of
625 functional stomata. *Nature Communications* **10**, 2825. (doi:10.1038/s41467-019-
626 10826-5)

627 43. Evans J, Vogelmann TC. 2003 Profiles of 14C fixation through spinach
628 leaves in relation to light absorption and photosynthetic capacity. *Plant, Cell &*
629 *Environment* **26**, 547–560.

630 44. West GB, Brown JH, Enquist BJ. 1999 A general model for the structure and
631 allometry of plant vascular systems. *Nature* **400**, 664–667.

632 45. Enquist BJ, Economo EP, Huxman TE, Allen AP, Ignace DD, Gillooly JF.
633 2003 Scaling metabolism from organisms to ecosystems. *Nature* **423**, 639.

634 46. Terashima I, Miyazawa S-I, Hanba YT. 2001 Why are Sun Leaves Thicker
635 than Shade Leaves? Consideration based on Analyses of CO_2 Diffusion in the
636 Leaf. *Journal of Plant Research* **114**, 93–105. (doi:10.1007/PL00013972)

637 47. Kozłowski J, Konarzewski M, Gawelczyk AT. 2003 Cell size as a link between
638 noncoding DNA and metabolic rate scaling. *Proceedings of the National*
639 *Academy of Sciences* **100**, 14080–14085. (doi:10.1073/pnas.2334605100)

640 48. Price CA *et al.* 2012 Testing the metabolic theory of ecology. *Ecology Letters*
641 **15**, 1465–1474. (doi:10.1111/j.1461-0248.2012.01860.x)

642 49. Leitch I, Bennett M. 2004 Genome downsizing in polyploid plants. *Biological*
643 *journal of the Linnean Society* **82**, 651–663.

644 50. Dodsworth S, Chase MW, Leitch AR. 2016 Is post-polyploidization
645 diploidization the key to the evolutionary success of the angiosperms? *Botanical*
646 *Journal of the Linnean Society* **180**, 1–5.

647 51. Levin DA. 1983 Polyploidy and novelty in flowering plants. *The American*
648 *Naturalist* **122**, 1–25.

649 52. Doyle JJ, Coate JE. 2019 Polyploidy, the nucleotype, and novelty: The impact
650 of genome doubling on the biology of the cell. *International Journal of Plant*
651 *Sciences* **180**, 1–52. (doi:10.1086/700636)

652 53. Baniaga AE, Marx HE, Arrigo N, Barker MS. 2020 Polyploid plants have
653 faster rates of multivariate climatic niche evolution than their diploid relatives.
654 *Ecology Letters* **23**.

655 54. Gürsoy D, De Carlo F, Xiao X, Jacobsen C. 2014 TomoPy: a framework for
656 the analysis of synchrotron tomographic data. *Journal of synchrotron radiation*
657 **21**, 1188–1193. (doi:10.1107/S1600577514013939)

658 55. Théroux-Rancourt G, Jenkins MR, Brodersen CR, McElrone A, Forrestel EJ,
659 Earles JM. 2020 Digitally deconstructing leaves in 3D using X-ray microcomputed

660 tomography and machine learning. *Applications in plant sciences* **8**, e11380.
661 (doi:10.1002/aps3.11380)

662 56. Borsuk, A. M., Roddy, A. B., Théroux-Rancourt, G. & Brodersen, C. R. 2019
663 Emergent honeycomb topology of the leaf spongy mesophyll. *bioRxiv*.
664 (doi:10.1101/852459)

665 57. Schneider CA, Rasband WS, Eliceiri KW. 2012 NIH Image to ImageJ: 25
666 years of image analysis. *Nature methods* **9**, 671–675.

667 58. Doube M, Kłosowski MM, Arganda-Carreras I, Cordelières FP, Dougherty
668 RP, Jackson JS, Schmid B, Hutchinson JR, Shefelbine SJ. 2010 BoneJ: Free
669 and extensible bone image analysis in ImageJ. *Bone* **47**, 1076–1079.
670 (doi:10.1016/j.bone.2010.08.023)

671 59. Leitch IJ, Johnston E, Pellicer J, Hidalgo O, Bennett MD. 2019. Plant DNA C-
672 values database (release 7.1, Apr 2019) https://cvalues.science.kew.org/

673 60. Dolezel J, Greilhuber J, Suda J. 2007 Estimation of nuclear DNA content in
674 plants using flow cytometry. *Nature Protocols* **2**, 2233–44.
675 (doi:10.1038/nprot.2007.310)

676 61. R Core Team. 2019 *R: A language and environment for statistical computing*.
677 Vienna, Austria: R Foundation for Statistical Computing. See https://www.R-
678 project.org/.

679 62. Warton DI, Duursma RA, Falster DS, Taskinen S. 2012 Smatr 3 - an r
680 package for estimation and inference about allometric lines. *Methods in Ecology
681 and Evolution* **3**, 257–259.